Cone-Beam Transmission Computed Tomography for Nonuniform Attenuation Compensation of SPECT Images

Stephen H. Manglos, Daniel A. Bassano, and F. Deaver Thomas

Department of Radiology, SUNY Health Science Center, Syracuse, New York

This paper develops and tests cone-beam transmission computed tomography (CB-CT) for attenuation compensation of SPECT images. CB-CT was implemented on a rotating gamma camera with a point source (1–2 mCi) of ^{99m}Tc, and a light-weight aluminum source holder. A cone-beam collimator may be used but is not required. Since the point source is either located at the collimator focal point, or the camera is uncollimated, CB-CT has excellent sensitivity (at least 150 times that of a parallel-hole, high-resolution collimator). The predicted resolution is equal to the intrinsic gamma camera resolution (3–4 mm), which is much higher than for a high-resolution, parallel-hole collimator (10–20 mm). In the present study, CB-CT provided low noise, high-resolution attenuation maps for use in a nonuniform attenuation-weighted backprojection algorithm. The attenuation compensation accuracy was tested using basic geometries of line sources and nonuniform density models. For the appropriate scaling of the attenuation map, the attenuation compensation was accurate and removed the SPECT image distortion associated with nonuniform attenuation. Attenuation maps acquired either with cone beam collimator or without any collimator were both successful. Using CB-CT, SPECT can thus be made much more accurate without adding unduly to the imaging time, complexity, or cost.

J Nucl Med 1991; 32:1813–1820

Quantification is potentially important in clinical single-photon emission computed tomography (SPECT) imaging. Some of the many possible applications include: calculations of activity density in μCi/ml or μCi/g (*1–2*), volume determination (*3*), myocardial perfusion analysis (*4–5*), receptor imaging (*6*), numerical analysis of brain perfusion (*7–9*), and liver imaging (*10*). Further, as SPECT becomes more accurate and new radiopharmaceuticals are developed, it seems likely that many additional applications will be developed, both for clinical imaging and biochemical research. Since photon attenuation is the major factor affecting SPECT image accuracy, it has been extensively studied. Compensation techniques have been developed (*11–25*) that have assumed a single uniform attenuation coefficient inside of a specified body contour. However, the true spatial distribution of attenuation coefficients (called the "attenuation map") is nonuniform, especially in the thorax and abdomen. Therefore, nonuniform attenuation has been studied (*10,14,26–30*) more recently, demonstrating that SPECT images are both quantitatively incorrect and spatially distorted, if they are uncompensated or if uniform attenuation compensation is applied.

Several nonuniform compensation methods have been developed, including Chang attenuation compensation with a nonuniform map (*14,28,29*), nonuniform attenuation-weighted backprojection (*26,31,32*), and nonuniform iterative maximum likelihood (*10,27,30,33*). All of these methods can compensate accurately for attenuation. The Chang method requires at least one iteration to remove the spatial distortion (*28*).

The major remaining factor blocking the routine implementation of these compensation methods is the lack of a convenient means of obtaining an accurate attenuation map. Previously, the attenuation map has been measured (*10,29,30,33,34*) with transmission radionuclide CT using a parallel-hole collimator and a sheet source attached to the rotating gamma camera normally used for SPECT. However, both the sensitivity and the spatial resolution are low so that at least 20 mCi of ^{99m}Tc and long acquisition times are required to obtain images which are still relatively noisy. If the sheet source is appropriately collimated, the photon scatter and dose to patient are reduced, but the added weight becomes difficult or impossible to support by many rotating gamma cameras. An alternative method is to transfer a conventional x-ray CT image to the computer used for SPECT reconstruction. For example, Singh et al. (*26*) successfully performed nonuniform attenuation compensation using data from a special focusing x-ray CT device (*35*). The conventional CT image of course has excellent quality, but the transfer and precise spatial alignment with the SPECT study can be difficult, time consuming, and subject to error. Further, not every patient has an appropriate CT available.

Recently, we proposed (36) a method, which uses cone-beam transmission radionuclide CT implemented on a rotating gamma camera to measure the attenuation map. For this method, an uncollimated point source is rotated in opposition to a gamma camera which is either uncollimated or has a cone-beam collimator. The cone beam acquisition geometry provides several important advantages, including maximum sensitivity, a light-weight easily-installed source, and high spatial resolution. The resolution is determined by the intrinsic camera resolution (3–4 mm), the point source size, and the pixel size, but *not* by the collimator resolution (10–20 mm). Cone-beam transmission reconstructions of test phantoms (36) showed good linearity of response as a function of attenuation coefficient, good spatial uniformity, and relatively low image noise even with a point source of only 200 μCi of ^{99m}Tc.

In consideration of the advantages of this method, this paper shows tests of attenuation compensation of SPECT phantoms, using attenuation maps obtained from cone-beam transmission CT (CB-CT). The accuracy of the compensation was checked by numerical measurements of the resulting SPECT images.

METHODS

Data Acquisition

Experimental phantoms were imaged sequentially with both parallel-ray SPECT and CB-CT using a Siemens Orbiter SPECT system and a ZLC-7500 gamma camera (Siemens Gammasonics, Hoffman Estates, IL). The following sequential order was used:

1. Align and position point source and test phantom (at this stage, the phantom had no radioactivity inside).
2. Perform CB-CT study with cone-beam collimator.
3. Perform CB-CT study without collimator.
4. Remove phantom, add radioactivity to the phantom, and reposition at same location.
5. Perform SPECT study with parallel-hole collimator.
6. Use the CB-CT reconstruction to provide attenuation compensation of the SPECT study.

Markers on the imaging table ensured that the phantom was in the same place for all studies. For human studies (not performed for this paper), the patient should be injected with the SPECT radiopharmaceutical after the CB-CT scan, if possible, and should remain motionless on the imaging table. Alternatively, simultaneous SPECT and CB-CT imaging must be developed.

Uniform and nonuniform cylinders were used as test phantoms. The nonuniform phantom approximated the thorax attenuation geometry, with lung and spine inserts, made of balsa wood and polyvinylidene fluoride respectively, placed in a circular 22-cm diameter cylinder which was otherwise filled with water. This geometry provided a good test of attenuation compensation in a nontruncated cone beam geometry.

For CB-CT acquisitions, the "point" sources were constructed by placing into a small cylindrical tube (6 mm diameter by 6 mm long) several drops of high concentration (about 100 mCi/ml) ^{99m}Tc sodium pertechnetate solution. The total activity was between 1 and 2 mCi of ^{99m}Tc, which is a factor of 10–100 lower than used previously in a sheet source (10,29,30,33,34). With

collimator, the observed count rate in the gamma camera for a 2-mCi point source and a uniform water-filled phantom was 70,000 cps with a dead time of 8%. Only second- or higher-order scatter was detected with collimator, so the scatter fraction must have been small. Without collimator, the observed count rate was 120,000 counts per second, with a dead time of 35%. The dead time was high partly because the amount of scatter was high. For the paralyzable ZLC-7500 counting system, higher source activities are inefficient, since the observed count rate would begin to decrease. In addition, a small amount of image degradation is possible at these high count rates. For example, the gamma camera manufacturer (Siemens Gammasonics, Hoffman Estates, IL) reports a negligible 0.2 mm spatial resolution loss and no uniformity loss at 70,000 cps. Energy resolution may also be degraded at these count rates.

The point source holder mass was only 3.5 kg. The holder was constructed of aluminum channel attached (see Fig. 1) to the gamma camera. The point source thus rotated with the gamma camera, but on the opposite side of the test phantom.

The CB-CT data were acquired either with cone-beam collimator (Van Mullekam—Nuclear Fields, Evanston, IL) or without any collimator whatsoever. In both cases, the geometry was cone beam, and the same point source location was used, specified by the focal point (at 54 cm) of the cone-beam collimator. The acquisition matrix was 64 × 64, with 64 angular views covering 360°. The acquisition time was about 10 min.

For the SPECT acquisitions, the ^{99m}Tc source activity was about 2 mCi for line sources and about 4 mCi for a uniform cylinder. All SPECT data were acquired with parallel-hole collimation. The acquisition matrices were either 64 × 64 with 64 views (for LEAP collimator) or 128 by 128 with 128 views (for HRES collimator).

Reconstruction Methods

The CB-CT reconstruction used a cone-beam filtered backprojection (37) algorithm. This algorithm is only an approximation, and the cone-beam geometry using a circle of source points does not provide a complete sampling of the image space (e.g., 38,39), but moderately accurate reconstructions were obtained (40–42) for cone-beam SPECT with similar cone angles. For our experiments, the geometry is fan beam for the central slice, where there is a complete sampling. We used only this central fan-beam slice
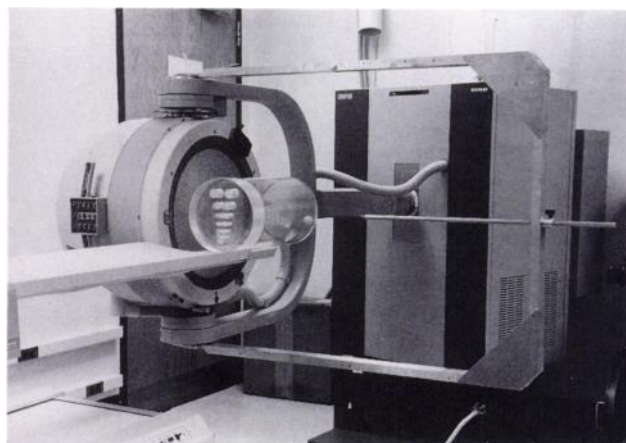

FIGURE 1. CB-CT acquisition with point source and holder, uncollimated gamma camera, and a test phantom.

for attenuation compensation, since it was appropriate for our cylindrically symmetric phantoms, and since outlying slices were truncated by the circular gamma camera field of view. Although iterative cone-beam reconstruction methods (39,43–48) exist and are more accurate, they require much longer execution times. We assumed that the increased accuracy was not necessary for the current experiment, although iterative algorithms may be preferred for the reconstruction of non-cylindrically-symmetric objects.

To process the observed transmission counts into an attenuation coefficient with correction for detection nonuniformities, a high-count "blank" acquisition (49) was acquired at a single view of the point source in air at the same location used for the CB-CT acquisition. This acquisition was denoted $N_o(i,j)$, where (i,j) are the digitized coordinates in the projection space. The blank acquisition was multiplicatively normalized to the CB-CT projections in an unattenuated region outside the object to be imaged. Next, the average line-integrated attenuation coefficient, $\mu_m(i,j)$, was calculated for each angle m using:

$$\mu_m(i,j) = -\ln[N_m(i,j)/N_o(i,j)].$$

The $N_m(i,j)$ are the measured CB-CT projection values. For those regions inside the square acquisition matrix but outside the circular active field of view of the detector, $\mu_m(i,j)$ was set directly to zero. It was discovered that the collimator masked out a significant portion of the gamma camera, reducing the effective active diameter by about 2.5 cm. Thus, the active region was larger without collimator than with collimator. The $\mu_m(i,j)$ were Hann-filtered, with a cut-off equal to the Nyquist frequency, and backprojected into a 64 × 64 reconstructed matrix with 32 slices. Due to cone-beam focusing, the image pixel size was reduced to about 4 mm, depending on the radius of rotation.

A nonuniform attenuation-weighted convolution and backprojection algorithm was used for reconstruction and attenuation compensation of the SPECT data. This "intrinsic" compensation method is an extension (31) of a uniform attenuation algorithm (19), and it is both fast and accurate, with good noise characteristics (19,50). A modified Shepp-Logan (19) convolution kernel was used. Again, iterative algorithms with a nonuniform map may be more accurate (10,27,30), but they require much longer computational times and thus were not investigated here.

Method of Analysis

For use in the SPECT reconstruction, one central CB-CT slice was scaled to an appropriate μ_{eff} in a known water-only region near the CB-CT image center. A major goal was to determine the optimal μ_{eff} giving the best attenuation compensation of the SPECT image. The accuracy of the attenuation compensation was measured using line spread functions, quantified as full-width at half- and tenth-maximum (FWHM, FWTM), in two orthogonal directions in a transverse slice. Also, the activity of compensated line sources was compared to the same sources imaged in air, with appropriate corrections for dead time and source decay. The total activity was calculated in a circular region of interest, with diameter equal to twice the FWTM. For a uniform activity, uniform density circular phantom, the desired uniformity of reconstruction was evaluated using narrow profiles through the image center.

RESULTS

Line Source Studies

A SPECT line source was imaged in the center of the nonuniform phantom and attenuation compensation was performed. The line source was also on the axis of rotation, to eliminate distortion due to the collimator response function. The CB-CT images used for attenuation compensation are shown in Figure 2, and were obtained both with a cone-beam collimator and without a collimator. Representative SPECT reconstructions are shown in Figure 3. As expected, the line reconstructed without attenuation compensation (i.e., $\mu_{eff} = 0$) was distorted into a roughly elliptical shape, elongated in the lateral direction, which was the direction of least attenuation (28). The attenuation compensation using either map (with or without a cone-beam collimator) improved the image, making the line source more circular. The measured FWHMs and FWTMs of the reconstructed line are given in Table 1, as a function of μ_{eff} used for scaling the attenuation map. The
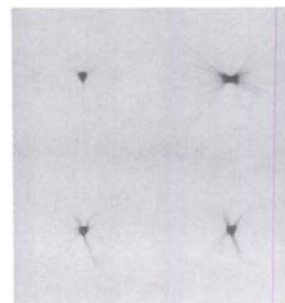
FIGURE 3. Representative transverse images of line source in thorax-simulating phantom. Full gray scale is at one-twentieth of the peak maximum to accentuate image distortion. Upper left is line source in air. Note small residual asymmetry. Upper right is line source in thorax phantom reconstructed without attenuation compensation. Note the roughly elliptical asymmetry. The reconstruction is longer in the lateral direction, and shorter in the anterior-posterior direction. Lower left is line source in thorax phantom with attenuation compensation using the attenuation map obtained *with* cone-beam collimator, scaled to the optimal coefficient ($\mu_{eff} = 0.13$ cm^{-1}). Lower right is line source in thorax phantom with attenuation compensation using the attenuation map obtained *without* cone-beam collimator, scaled to the optimal coefficient ($\mu_{eff} = 0.12$ cm^{-1}).
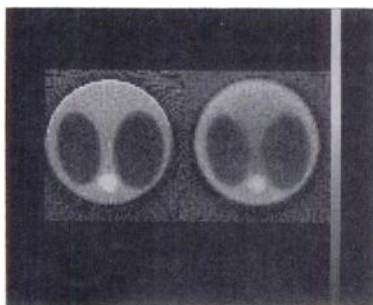

FIGURE 2. CB-CT transverse slices of nonuniform phantom. (Left) With cone-beam collimator, (Right) without collimator. These attenuation maps were used for attenuation compensation of the SPECT line source data.

TABLE 1
Line in Circular Nonuniform Phantom: Compensation Using CB-CT with Cone-Beam Collimator

μ_{eff} (cm⁻¹)	Right-Left		Anterior-Posterior		RFWHM*	RFWTM†
	FWHM	FWTM	FWHM	FWTM		
0.00 (no comp)	13.6	27.6	10.3	17.0	1.32	1.62
0.09	12.0	23.2	11.2	19.5	1.07	1.19
0.10	11.8	22.7	11.3	20.0	1.04	1.14
0.11	11.6	22.2	11.5	20.3	1.01	1.09
0.12	11.5	21.6	11.6	20.8	0.99	1.04
0.13	11.3	20.9	11.8	21.2	0.96	0.99
0.14	11.2	20.3	11.9	21.6	0.94	0.94
0.15	11.0	19.9	12.1	22.2	0.91	0.90
Compensation Using CB-CT Without Cone-Beam Collimator						
0.06	12.4	24.0	10.9	18.6	1.14	1.29
0.07	12.2	23.5	11.0	19.0	1.11	1.24
0.08	12.0	23.0	11.1	19.4	1.08	1.19
0.09	11.8	22.5	11.3	19.8	1.04	1.14
0.10	11.6	21.8	11.4	20.2	1.02	1.08
0.11	11.4	21.2	11.6	20.6	0.98	1.03
0.12	11.3	20.5	11.7	21.0	0.97	0.98
0.13	11.1	20.0	11.9	21.5	0.93	0.93
0.14	10.9	19.5	12.1	22.1	0.90	0.88
0.15	10.8	18.9	12.2	22.8	0.89	0.83
Line in air	11.6	20.7	12.0	21.0	0.97	0.99

*RFWHM = Ratio of right-to-left FWHM to anterior-to-posterior FWHM.

†RFWTM = Ratio of right-to-left FWTM to anterior-to-posterior FWTM.

full-widths are given in the two orthogonal directions which give the largest and the smallest full-widths (the long- and short-axes of the elliptical distortion). Without attenuation compensation, the reconstructed ellipse long-axis-to-short-axis ratio was large: 1.3 at the half-maximum and 1.6 at the tenth-maximum. With attenuation compensation, these ratios were much closer to the desired value of 1.0. The optimal attenuation coefficient for scaling of the CB-CT attenuation map was defined as that for which the full-widths most nearly equaled those obtained for the line in air. For the map obtained with a cone-beam collimator, the optimal value averaged over the four full-width measurements for each μ_{eff} was 0.129 cm⁻¹ with a measured spread (standard deviation) over the four measurements of 0.012 cm⁻¹. For the map obtained without a cone-beam collimator, the optimal μ_{eff} was 0.118 cm⁻¹ with a measured spread over the four measurements of 0.014 cm⁻¹.

The reconstructed line in air itself had some residual asymmetry. Its cause is unknown, but the asymmetry was seen with or without center of rotation correction. In fact, the dependence on center of rotation correction was insignificant, since the gamma camera had been tuned to give a small measured correction of less than 1 mm. The dependence on slice, which gives an upper bound on the

statistical error, was small. Over eight slices measured, the variation of the full-widths with slice was no more than 0.3 mm. For each slice the asymmetry was similar in appearance and size (FWHM, FWTM). Although we defined our optimal coefficient to be that which gave agreement with the reconstructed line in air instead of perfect symmetry of reconstruction (i.e.: ratios equal to 1.0 in Table 1), the value of μ_{eff} giving most perfect symmetry was always within 0.01 cm⁻¹ of the value giving agreement with the line source in air.

For the same line sources, the total reconstructed activity was compared to the reconstructed activity in air. Figure 4 shows that the reconstructed activity equaled the "in air" activity when μ_{eff} was set to 0.129 cm⁻¹ and the attenuation map was obtained with a cone-beam collimator. For the map obtained without a collimator, a μ_{eff} of 0.091 cm⁻¹ gave agreement with the "in air" activity. The third digit to the right of the decimal point in these measurements was estimated using linear interpolation.

A similar experiment was done with the line source centered in a uniform density cylinder. The ratio of attenuation compensated activity to "in air" activity is given in Figure 5. The ratio was 1 for μ_{eff} = 0.138 cm⁻¹ and the attenuation map obtained with a cone-beam collimator. For the map obtained without collimator, a μ_{eff} of 0.125 cm⁻¹ gave a ratio of 1. Since the line was centered in a uniform circular cylinder, the attenuation was isotropic, and thus insignificant reconstruction asymmetry was observed.

Uniform Activity Studies

Attenuation compensation of uniform radioactivity in a uniform density circular cylindrical phantom provided an additional test of the method's accuracy. In Figures 6 and 7 representative profiles through the center of the images with representative scaling coefficients are shown. For a map with a cone-beam collimator, a flat, uniform reconstruction was obtained with a μ_{eff} of about 0.11 cm⁻¹. For a map without a cone-beam collimator, a flat reconstruction was obtained with μ_{eff} of about 0.12 cm⁻¹.
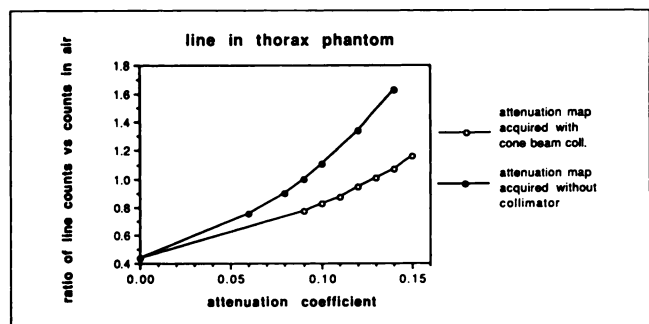

FIGURE 4. The activity ratio of attenuation compensated line in thorax phantom versus line in air. A ratio of 1 indicates accurate attenuation compensation. Open and solid circles are attenuation maps obtained with and without a cone-beam collimator, respectively.
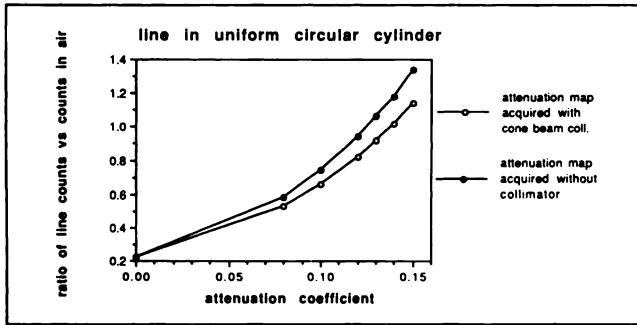
FIGURE 5. The activity ratio of attenuation compensated line in uniform circular phantom versus line in air. A ratio of 1 indicates accurate attenuation compensation. The open and solid circles are attenuation maps obtained with and without a cone-beam collimator, respectively.

Sensitivity Measurement

Simple sensitivity measurements were made for the two CB-CT geometries with the circular thorax phantom in place. The measurements were compared to the sensitivity for a high-resolution (HRES) collimator on the camera, measured with the same point source location in all cases. The CB-CT sensitivity with a collimator was 170 times that of the HRES collimator. Without a collimator, the sensitivity was 440 times that of the HRES collimator. Therefore, any transmission CT measurement with a HRES collimator will require much higher source activity or much longer acquisition time, with a corresponding increase in exposure to the patient and the technologist, to give the same noise level as with CB-CT.

Additionally, these data indicate that the sensitivity without a collimator is 2.6 times that with a cone-beam collimator, due in part to scatter from the intervening phantom. Without a phantom in place, and thus without photon scatter, the sensitivity without a collimator (680 cps/μCi) was 2.0 times the sensitivity with a cone-beam collimator (340 cps/μCi). Therefore, an approximation for

FIGURE 6. Profiles through center of transverse images of uniform activity, uniform density, and circular phantom. Attenuation map was obtained *with* cone-beam collimator. The values of μ_{eff} used for scaling are indicated for each curve in units of cm^{-1}.
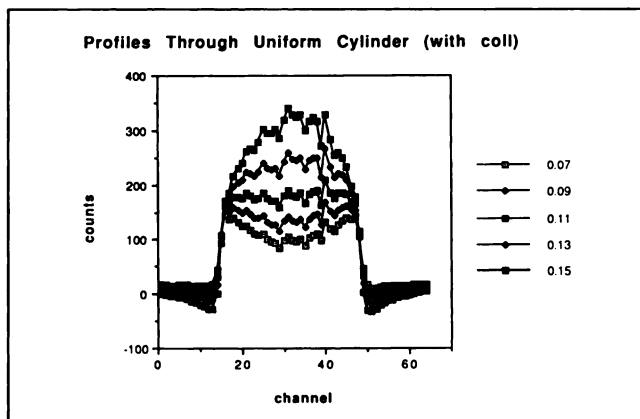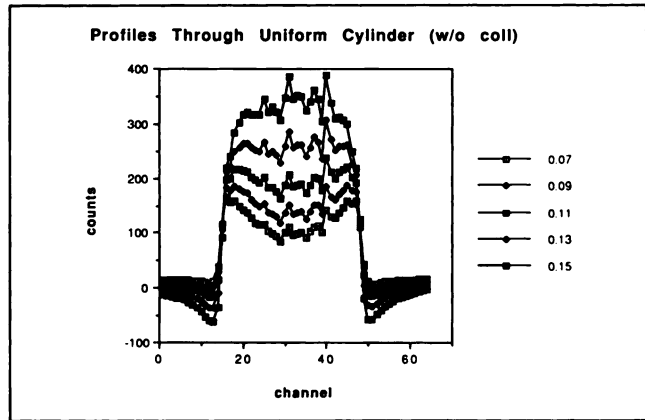

FIGURE 7. Profiles through center of transverse images of uniform activity, uniform density, and circular phantom. Attenuation map was obtained *without* cone-beam collimator. The values of μ_{eff} used for scaling are indicated for each curve in units of cm^{-1}.

the scatter fraction obtained without a collimator and with a phantom is:

$$(2.6 - 2.0)/[1 + (2.6 - 2.0)] = 0.6/1.6 = 0.38,$$

neglecting the small amount of higher-order scattering with cone beam collimator.

It is surprising that there is a large difference in sensitivity "with" versus "without" collimator when no phantom (or scatter) is present, since theoretically for this geometry all septa are illuminated edge on. The theoretical sensitivity ratio, assuming proper collimator construction, is directly calculable from the total detector surface area illuminated by the point source:

$$R_{sens} = (\text{sensitivity without collimator})/$$
$$(\text{sensitivity with cone-beam collimator}) \quad \text{Eq. 1}$$
$$= \pi(d + t)^2 N/\pi d^2 N,$$

where N = the number of holes. For our collimator, the hole size d is 1.8 mm, the septal thickness t is 0.25 mm, and R$_{sens}$ should be 1.30, instead of 2.0. A detailed evaluation of this collimator suggests that the explanation of the high measured ratio is collimator imperfection: the holes do not all focus to the nominal focal point, and thus many or most septa are not illuminated edge on. Thus, the "effective" septal thickness (t$_{eff}$) is much larger, for the given source location and the septal angulation error. To get R$_{sens}$ equal to 2.0 in Equation 1 would require t = t$_{eff}$ = 0.75 mm, which is three times the nominal septal thickness. However, this implies an average septal angulation error of only about 1°. A complete analysis of our cone-beam collimator and the effects of collimator nonuniformity has been performed and is being prepared for publication (51).

DISCUSSION

This study has provided both a reiteration of previous results regarding nonuniform attenuation and new results

specific to the use of CB-CT for attenuation map measurement. This study has redemonstrated that, in general, a nonuniform attenuation map is necessary for accurate attenuation compensation and to remove the SPECT image distortion which is otherwise present. This necessity is especially true for the imaging of line sources in geometries like the human thorax. We expect that nonuniform attenuation compensation is also important *clinically* (e.g., human myocardial imaging) (*30*). However, the application of CB-CT to humans or large phantoms is complicated and will require both longer focal lengths (e.g., at least 100 cm) and an evaluation of possible truncation artifacts. Our preliminary work with human chest imaging (*52*) indicated that truncation artifacts will be large for some patients imaged on standard large field of view gamma cameras. Either larger gamma cameras, commercially available now in rectangular shape with widths up to 61 cm, or image processing methods (*21,53–58*) will be necessary to reduce the artifacts.

For the present work, CB-CT has been shown to provide an attenuation map which gives accurate nonuniform attenuation compensation. The CB-CT image quality, with low noise and high spatial resolution, is dramatically superior (Fig. 2) to images obtainable with a sheet source. The compensation was evaluated in the fundamental and essential geometry of line sources in a nonuniform thorax-simulating phantom. Only a central (fan-beam) slice of the CB-CT data was used for attenuation compensation, since the circular gamma camera produced truncation in most other slices for this geometry. Apart from truncation effects, other studies (*36,52*) demonstrated satisfactory images for these outlying slices, and therefore we expect, but have not demonstrated, accurate attenuation compensation using the outlying slices. However, the cone-beam geometry does not completely sample these slices, thus producing an error which has not yet been quantitatively evaluated.

The accuracy of the compensation depends on the scaling of the attenuation map, but reasonable scalings (with an attenuation coefficient, μ_{eff}, near 0.12 cm^{-1}) provide accurate compensations. For our tests the scaling was applied in terms of a known water region in the center of a phantom. Although for human SPECT, known water density regions do not exist, scaling the attenuation map for humans should be easy to develop.

The optimal scaling of the attenuation map, giving most accurate attenuation compensation of SPECT phantom images, was determined for several geometries as a value of μ_{eff}. For an attenuation map acquired with a cone-beam collimator, the optimal μ_{eff} ranged from 0.11–0.14 cm^{-1} for the test geometries. The data are summarized in Table 2. Most likely, any μ_{eff} in this range will give accurate enough attenuation compensation for typical applications. Accurate attenuation compensation is also possible using a map acquired without any collimator. The detection geometry is still cone beam. Without a collimator, the

TABLE 2
Optimal μ_{eff} Summary

Type of measurement	μ_{eff} (cm^{-1})
With cone-beam collimator	
Line shape in thorax phantom	0.129
Line activity in thorax phantom	0.129
Line activity in uniform phantom	0.138
Uniform activity: uniformity of reconstruction	0.11
Without collimator	
Line shape in thorax phantom	0.118
Line activity in thorax phantom	0.091
Line activity in uniform phantom	0.125
Uniform activity: uniformity of reconstruction	0.12

optimal μ_{eff} ranged from 0.09–0.12 cm^{-1} for the test geometries. These values were lower than the "with collimator" values, due to scatter, which makes the center of the CT image appear less dense than the edge. If scatter correction were applied to the "without collimator" CT acquisitions, the μ_{eff}'s would be closer to the "with collimator" values.

The optimal μ_{eff} for attenuation compensation may depend on the compensation algorithm used. We used an attenuation-weighted backprojection method (*19*) modified (*31*) for nonuniform attenuation. If another algorithm is to be used, the optimal μ_{eff} should be retested.

Since photon scatter was also present in the *SPECT* acquisitions, but no separate scatter compensation was performed, the optimal μ_{eff} values were close to the previously-measured broad beam coefficient (*59*) (0.11–0.12 cm^{-1} for water). If scatter compensation were applied to the SPECT study, the optimal μ_{eff}'s for attenuation compensation would be closer to the narrow beam μ of 0.15 cm^{-1} for water.

The spread in the μ_{eff}'s as a function of measurement was significant (Table 2). For example, in the measurement of a uniform circular cylinder, the "without collimator" data seemed to suggest a μ_{eff} higher than "with collimator," with flatness of reconstruction as the criterion. This was contrary to expectations, since the scaling is performed in the image center, and while the "with collimator" map was nearly uniform throughout, the "without collimator" map was lowest at the center and higher elsewhere, due to photon scatter. Thus, the "without collimator" map should have provided more correction for a given μ_{eff}, and the optimal value should be lower. Careful study of Figure 7 (without collimator) indicates that in terms of CT value, the optimal reconstruction did not give a flat profile. For example, using a μ_{eff} of 0.107 cm^{1-} in the compensation without collimator gives SPECT activity in the phantom center which is equal to using μ_{eff} = 0.11 cm^{-1} in the compensation with collimator. However, this attenuation coefficient (0.107 cm^{-1}) does not give a flat SPECT profile. Using a higher μ_{eff} to give a flat profile will overcorrect the

SPECT activity, relative to the "with collimator" case. Thus, flatness is not a complete measure of reconstruction accuracy.

Some possible sources of inaccurate reconstruction include photon scatter and image noise, in both the CB-CT and the SPECT data, and the attenuation compensation algorithm. This experiment does not determine separately the effect of each possible source of error, but the high overall accuracy suggests that the individual effects are small. The noniterative attenuation compensation algorithm that was used is relatively fast and has been previously evaluated in detail (19,31,50). Nonetheless, it is probable that higher accuracy and more consistent results will be obtained with scatter corrections and an accurate iterative attenuation compensation algorithm (10,27,30).

Some small uncertainty (no more than 0.01 cm^{-1}) was present in the line source measurements of optimal μ_{eff}, as a result of the slight but unexplained asymmetry of the line source in air reconstructions. Different but still significant line source reconstruction asymmetry has also been seen using our Triad SPECT camera (Trionix Research Laboratory), suggesting that imperfect line source reconstructions may be common. Existing center of rotation corrections were unable to remove these small asymmetries. The asymmetries were similar from slice to slice, suggesting that the asymmetry is not a result of noise in the projections.

CONCLUSION

Coupled with previous work discussing the dramatically superior sensitivity and spatial resolution (36), the current work suggests that CB-CT may become the best method for obtaining the attenuation map necessary for accurate quantification of SPECT images. Accurate attenuation compensation has now been demonstrated for reasonable attenuation map scalings. The high sensitivity, which is at least 150 times higher than for CT with a sheet source, and the resulting reduced acquisition times may make routine quantitative SPECT possible. In addition, the predicted spatial resolution is about 3 mm for CB-CT versus 10–20 mm for CT with a sheet source. The high-quality attenuation map may also be useful for accurate scatter compensation methods using a nonuniform map (22,60). Further, automatically-aligned functional (SPECT) and anatomical (CB-CT) correlated imaging will be possible. Clearly, additional improvements in detector design, including higher resolution and count rate, and larger size, would be very useful for this application.

REFERENCES

1. Caldwell JH, Williams DL, Hamilton GW, et al. Regional distribution of myocardial blood flow measured by single-photon emission tomography: comparison with in vitro counting. J Nucl Med 1982;23:490–495.
2. Kircos LT, Carey JE, Keyes JW. Quantitative organ visualization using SPECT. J Nucl Med 1987;28:334–341.
3. Tauxe WN, Soussaline F, Todd-Pokropek A, et al. Determination of organ volume by single-photon emission tomography. J Nucl Med 1982;23:984–987.

4. Garcia EV, Van Train K, Maddahi J, et al. Quantification of rotational thallium-201 myocardial tomography. J Nucl Med 1985;26:17–26.
5. Maddahi J, Van Train KF, Prigent F, et al. Quantitation of T1-201 myocardial single-photon emission computerized rotational tomography: development, validation, and prospective application of an optimized computerized method [Abstract]. J Nucl Med 1986;27:899.
6. Kilbourn MR, Zalutsky MR. Research and clinical potential of receptor based radiopharmaceuticals. J Nucl Med 1985;26:655–662.
7. Cohen MB, Lake RR, Graham LS, et al. Quantitative iodine-123-IMP imaging of brain perfusion in schizophrenia. J Nucl Med 1989;30:1616–1620.
8. Maurer AH, Siegel JA, Comerota AJ. SPECT quantification of cerebral ischemia before and after carotid endarterectomy. J Nucl Med 1990;31:1412–1420.
9. Gemmell HG, Evans NTS, Besson JAO, et al. Regional cerebral blood flow imaging: a quantitative comparison of technetium-99m-HMPAO SPECT with C^{15}O$_2$ PET. J Nucl Med 1990;31:1595–1600.
10. Malko JA, Van Heertum RL, Gullberg GT, Kowalsky WP. SPECT liver imaging using an iterative attenuation correction algorithm and an external flood source. J Nucl Med 1986;27:701–705.
11. Kay DB, Keyes JW. First-order corrections for absorption and resolution compensation in radionuclide Fourier tomography. J Nucl Med 1975;16:540–541.
12. Keyes JW, Orlandea N, Heetderks WJ, Leonard PF, Rogers WL. The humongotron: a scintillation-camera transaxial tomograph. J Nucl Med 1977;18:381–387.
13. Budinger TF, Derenzo SE, Gullberg GT, Greenberg WL, Huesman RH. Emission computed assisted tomography with single-photon and positron annihilation photon emitters. J Comp Assist Tomog 1977;1:131–14.
14. Chang L-T. A method for attenuation correction in radionuclide computed tomography. IEEE Trans Nucl Sci 1978;25:638–643.
15. Tretiak O, Metz C. The exponential radon transform. SIAM J Appl Math 1980;39:341–354.
16. Gullberg GT, Budinger TF. The use of filtering methods to compensate for constant attenuation in single-photon emission computed tomography. IEEE Trans Biomed Eng 1981;28:142–157.
17. Walters TE, Simon W, Chesler DA, Correia JA. Attenuation correction in gamma emission computed tomography. J Comp Assist Tomog 1981;5:89–94.
18. Tanaka E. Quantitative image reconstruction with weighted backprojection for single photon emission computed tomography. J Comp Assist Tomog 1983;7:692–700.
19. Tanaka E, Toyama H, Murayama HE. Convolutional image reconstruction for quantitative single photon emission computed tomography. Phys Med Biol 1984;29:1489–1500.
20. Kim KI, Tewarson RP, Bizais Y, Rowe RW. Inversion for the attenuated Radon transform with constant attenuation. IEEE Trans Nucl Sci 1984;31:538–542.
21. Gullberg GT, Huesman RH, Malko JA, Pelc NJ, Budinger TF. An attenuated projector-backprojector for iterative SPECT reconstruction. Phys Med Biol 1985;30:799–816.
22. Floyd CE, Jaszczak RJ, Coleman RE. Inverse Monte Carlo: a unified reconstruction algorithm for SPECT. IEEE Trans Nucl Sci 1985;32:779–785.
23. Floyd CE, Jaszczak RJ, Greer KL, Coleman RE. Inverse Monte Carlo as a unified reconstruction algorithm for ECT. J Nucl Med 1986;27:1577–1585.
24. Larsson SA. Gamma camera emission tomography. Acta Radiol 1980;363(suppl):28–32.
25. Bellini S, Piacentini M, Cafforio C, Rocco F. Compensation of tissue absorption in emission tomography. IEEE Trans Acoustics, Speech, and Signal Proc 1979;27:213–218.
26. Singh M, Berggren MJ, Gustafson DE, Dewanjee MK, Bahn RC, Ritman EL. Emission-computed tomography and its application to imaging of acute myocardial infarction in intact dogs using Tc-99m-pyrophosphate. J Nucl Med 1979;20:50–56.
27. Miller MI, Snyder DL, Miller TR. Maximum-likelihood reconstruction for single-photon emission computed-tomography. IEEE Trans Nucl Sci 1985;32:769–778.
28. Manglos SH, Jaszczak RJ, Floyd CE, Hahn LJ, Greer KL, Coleman RE. Non-isotropic attenuation in SPECT: phantom tests of quantitative effects and compensation techniques. J Nucl Med 1987;28:1584–1591.
29. Bailey DL, Hutton BF, Walter PJ. Improved SPECT using simultaneous emission and transmission tomography. J Nucl Med 1987;28:844–851.
30. Tsui BMW, Gullberg GT, Edgerton ER, et al. Correction of nonuniform

attenuation in cardiac SPECT imaging. *J Nucl Med* 1989;30:497–507.

31. Manglos SH, Jaszczak RJ, Floyd CE. Weighted backprojection implemented with a non-uniform attenuation map for improved SPECT quantitation. *IEEE Trans Nucl Sci* 1988;35:625–628.

32. Singh M, Horne M, Maneval D, Amartey J, Brechner R. Nonuniform attenuation and scatter correction in SPECT. *IEEE Trans Nucl Sci* 1988;35:767–771.

33. Tsui BMW, Hu G-B, Gilland DR. Implementation of simultaneous attenuation and detector response correction in SPECT. *IEEE Trans Nucl Sci* 1988;35:778–783.

34. Greer KL, Harris CC, Jaszczak RJ, Coleman RE, Floyd CE, Manglos SH. Transmission computed tomography data acquisition with a SPECT system. *J Nucl Med Technol* 1987;15:53–56.

35. Sturm RE, Ritman EL, Johnson SA, Wondrow MA, Erdman DI, Wood EH. Prototype of a single x-ray video imaging chain designed for high temporal resolution computerized tomography by means of an electronic scanning dynamic spatial reconstruction system. In: *Proceedings San Diego Biomedical Symposium*. New York: Academic Press; 1976;15:181–189.

36. Manglos SH, Bassano DA, Duxbury CE, Capone RB. Attenuation maps for SPECT determined using cone beam transmission computed tomography. *IEEE Trans Nucl Sci* 1990;37:600–608.

37. Feldkamp LA, Davis LC, Kress JW. Practical cone beam algorithm. *J Opt Soc Am A* 1984;1:612–619.

38. Smith BD. Cone Beam tomography: recent advances and a tutorial review. *Opt Eng* 1990;29:524–534.

39. Zeng GL, Gullberg GT. A study of reconstruction artifacts in cone beam tomography using filtered backprojection and iterative EM algorithms. *IEEE Trans Nucl Sci* 1990;37:759–767.

40. Jaszczak RJ, Floyd CE, Manglos SH, Greer KL, Coleman RE. Cone-beam collimation for single photon emission computed tomography: analysis, simulation, and image reconstruction using filtered backprojection. *Med Phys* 1986;13:484–489.

41. Jaszczak RJ, Greer KL, Coleman RE. SPECT using a specially designed cone-beam collimator. *J Nucl Med* 1988;29:1398–1405.

42. Manglos SH, Jaszczak RJ, Greer KL. Cone beam SPECT reconstruction with camera tilt. *Phys Med Biol* 1989;34:625–631.

43. Floyd CE, Jaszczak RJ, Greer KL, Coleman RE. Cone-beam collimation for SPECT: simulation and reconstruction. *IEEE Trans Nucl Sci* 1986;33:511–514.

44. Manglos SH, Jaszczak RJ, Floyd CE. Maximum Likelihood reconstruction for cone beam SPECT: development and initial tests. *Phys Med Biol* 1989;34:1947–1957.

45. Manglos SH, Jaszczak RJ, McAfee JG. Maximum likelihood reconstruc-

tion for cone beam SPECT with camera tilt. *IEEE Trans Nucl Sci* 1989;36:1117–1121.

46. Gullberg GT, Zeng GL, Tsui BMW, Hagius JT. An iterative reconstruction algorithm for single photon emission computed tomography with cone beam geometry. *J Imag Sys Tech* 1989;1:169–186.

47. Gullberg GT, Zeng GL, Christian PE, Tsui BMW, Morgan HT. Single photon emission computed tomography of the heart using cone beam geometry and noncircular detector rotation. In: Ortendahl DA, Llacer J, eds. *Information processing in medical imaging, XIth IPMI international conference*. New York: Wiley-Liss; 1989:123–138.

48. Hu H, Gullberg GT. Quantitative cone-beam reconstruction. *SPIE Medical Imaging II* 1989;1092:492–501.

49. Ljungberg, Strand S-E. Attenuation correction in SPECT based on transmission studies and Monte Carlo simulations of build-up functions. *J Nucl Med* 1990;31:493–500.

50. Manglos SH, Jaszczak RJ, Floyd CE, Hahn LJ, Greer KL, Coleman RE. A quantitative comparison of attenuation-weighted backprojection with multiplicative and iterative postprocessing attenuation compensation in SPECT. *IEEE Trans Med Imag* 1988;7:127–134.

51. Manglos SH, Capone RB, Bassano DA. Detection uniformity measurements and corrections for cone beam transmission CT. *Med Phys* 1991: in press.

52. Manglos SH, Bassano DA, Thomas FD, Grossman ZD. Cone beam transmission CT of human subjects. *Radiology* 1991;177(P):169.

53. Shepp LA, Vardi Y. Maximum likelihood reconstruction for emission tomography. *IEEE Trans Med Imag* 1982;1:113–132.

54. Lange K, Carson R. EM reconstruction algorithms for emission and transmission tomography. *J Comp Assist Tomogr* 1984;8:306–316.

55. Herman GT, Lewitt RM. Evaluation of a preprocessing algorithm for truncated CT projections. *J Comp Assist Tomogr* 1981;5:127–135.

56. Tung C, Gullberg GT, Tsui BMW, Perry JR. Reconstruction of truncated fan beam data of the heart [Abstract]. *J Nucl Med* 1989;30:755.

57. Ogawa K, Nakajima M, Yuta S. A reconstruction algorithm from truncated projections. *IEEE Trans Med Imag* 1984;MI-3:34–40.

58. Chang L-T. Attenuation correction and incomplete projection in single photon emission computed tomography. *IEEE Trans Nucl Sci* 1979;NS-26:2780–2789.

59. Harris CC, Greer KL, Jaszczak RJ, Floyd CE, Fearnow EC, Coleman RE. Tc-99m attenuation coefficients in water-filled phantoms determined with gamma cameras. *Med Phys* 1984;11:681–685.

60. Mukai T, Links JM, Douglass KH, Wagner Jr HN. Scatter correction in SPECT using non-uniform attenuation data. *Phys Med Biol* 1988;33:1129–1140.